High Resolution Thermal Imaging of Pre-Breakdown in Power AlGaN/GaN MOSHEMTs

Kerry Maize, Hong Zhou, Peide D. Ye, Ali Shakouri
Birck Nanotechnology Center, Purdue University, West Lafayette, IN 47906, USA
Email: kmaize@purdue.edu

***Abstract*—Thermoreflectance imaging microscopy is demonstrated for pre-breakdown thermal and material analysis of power AlGaN/GaN MOSHEMTs stressed to catastrophic breakdown. Optical and thermal images with submicron spatial resolution reveal evolution of self-heating and mechanical degradation on the MOSHEMT gate metal for both the full-ON and full-OFF operating states, with V_D up to 155 V. Strong correlation was observed between localized hot spots/cold spots under bias and material breakdown at the fail site. Results demonstrate rapid quantitative in situ imaging of HEMT pre-breakdown phenomena with broad implications for reliability and design optimization.**

***Index Terms*—Power transistors, HEMTs, Semiconductor device breakdown, Thermal stresses**

I. Introduction

Catastrophic breakdown in integrated electronics is a major reliability concern. Before the breakdown, irregular temperature distribution under bias can reveal areas of increased local stress. At sufficient power, thermal runaway at defect sites can lead to breakdown. Analysis of catastrophic breakdown is challenging because it is quite sudden and it can have multiple causes (e.g.: defects in the material or during the fabrication of bulk or fabrication defects). Post failure inspection, such as SEM, does not provide critical information preceding breakdown. Electrical characterization describes performance before and up to breakdown, but it is based on overall behavior of the device and does not include important thermal information. Individual temperature sensors such as thermistors or embedded diodes are constrained in spatial resolution and may not identify critical hot spots that eventually lead to breakdown.

Here we demonstrate thermoreflectance imaging microscopy [1], [2] of power AlGaN/GaN MOSHEMTs stressed to breakdown. High resolution thermal images reveal localized hot spots and cold spots over the full range of the stress cycle, from low bias up to catastrophic breakdown. Direct correlation is observed between localized hot/cold spots during operation and material breakdown at the fail site. Quantitative, rapid in situ inspection of temperature distribution in relation to catastrophic device breakdown assists study of underlying thermal mechanisms and facilitates simulation, design and process optimization.

A. Device description

Fig. 1 shows the test structures. Multifinger GaN MOSHEMTs were based on a novel ALE grown single crystalline MgCaO gate dielectric to suppress gate leakage. [3], [4]

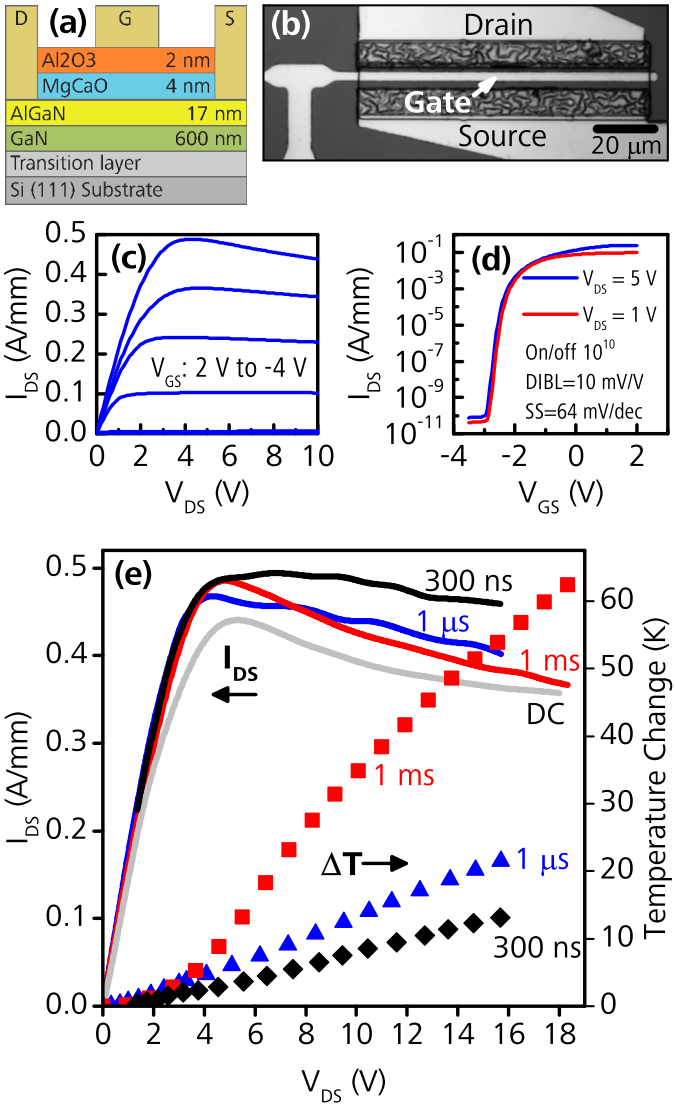

Fig. 1. MgCaO gate dielectric AlGaN/GaN power MOSHEMT. (a) Schematic cross section of MOSHEMT stack. (b) Microscope optical image of the top of the MOSHEMT. Gate width is 100 microns, gate length is five microns. (c) and (d) DC electrical characteristics. Gate length is eight microns. (e) I_D and self-heating dependence on drain voltage pulse width for MOSHEMT shown in (b). Gate voltage is constant, V_G = +2.0 V. Temperature change is sampled on gold gate metal.

Fig. 1 (a) shows the schematic cross section of the MOSHEMT stack with ultra-thin MgCaO oxide gate dielectric. This MOS

gate has been shown to reduce gate leakage compared to conventional Schottky gates common in many GaN HEMTs while still achieving very good switching performance. Drain, source, and gate contacts are gold. Fig. 1 (b) shows top view layout of the MOSHEMT. Gate width is 100 microns for all devices in this study. Gate length varies from 4.75 microns to 40 microns. Gate length for the device in (b) is 5 microns. All thermoreflectance images in this study measured temperature on the top of the gate metal, and all stated lengths refer to this dimension as viewed from the top. Fig. 1 (c) and (d) plot the DC electrical performance of an identical device with gate length of eight microns. It is worth noting in (c) the decrease in current at higher applied power due to device self-heating. This so-called "thermal droop" is well known and intrinsic to most power applications and this paper includes thermoreflectance image results correlating MOSHEMT temperature and current degradation. However, the purpose of this study is to explore the role of temperature not in the stable device operating regime, but as a precursor and eventual cause of catastrophic device breakdown.

B. Methods

Thermoreflectance imaging microscopy measures temperature dependent change in sample material reflectance during self-heating. This reflectance change is small, on the order of 10^{-5} to 10^{-3} per degree Celsius, and measurement with good resolution requires averaging the reflectance change using synchronous lock-in excitation. The device under test is electrically excited by continuous pulsed voltage synchronized to image acquisition using a high dynamic range CCD camera. Full field of view microscope images of device heating with 50 milliKelvin temperature resolution can be achieved in five minutes averaging. Spatial resolution is diffraction limited, or approximately 250 nanometers using visible wavelength illumination. Thermoreflectance imaging was performed using a modified Microsanj NT 200t system. Thermoreflectance images of HEMT self heating distribution were averaged for ten minutes at each bias point. Devices were probed on wafer, with substrate affixed to large copper heat sink maintained at room temperature.

During thermoreflectance imaging measurement the MOSHEMTs are excited by low duty cycle voltage pulses. For each image in this study the drain was pulsed while gate voltage was held constant, though the reverse configuration is also feasible to inspect transistor self-heating. Each image is acquired using a selected pulse voltage amplitude and time duration. Pulse duty cycle is 10 % for all images. Pulse width chosen within the range 300 nanoseconds to five milliseconds. Although thermoreflectance imaging requires excitation using a pulse waveform, device performance at electrical and thermal steady state can be probed by using a waveform whose pulse width is longer than the device thermal rise time. This effective steady state pulse width can be determined by transient thermoreflectance measurement, or by choosing a pulse width that reproduces the steady state I_D-V_D curve. The latter approach is illustrated in Fig. 1 (e) which shows MOSHEMT drain current for V_D pulses of 300 nanoseconds, one microsecond, and one millisecond, all using 10% duty cycle. Corresponding thermoreflectance temperature change sampled on the gold gate metal for the three different pulse widths are also shown. We observe self heating increase with longer pulse duration and an inverse relation between temperature and drain current. This trend matches the thermal droop evident in separate steady state electrical measurement shown in both Fig. 1 (c) and (e). Thermoreflectance pulse width of one millisecond closely reproduces the DC response, and this pulse width was used for all breakdown measurement of the MOSHEMT unless indicated otherwise. The remainder of this paper examines MOSHEMT spatial thermal characteristics, highlighting observed correlation between MOSHEMT local thermal features and apparent fail sites during pre-breakdown and eventual catastrophic breakdown. All subsequent thermoreflectance images of the MOSHEMT were obtained using bias pulses of one millisecond duration to reproduce effective thermal steady state. Transient or faster pulsed thermal effects are reserved for a future study.

II. Results

Breakdown stress bias was applied by increasing drain voltage linearly from 0 V to $V_{breakdown}$ while holding gate voltage constant. HEMT breakdown was inspected for ON and OFF channel conductivity states. Full ON (V_G = +2.0 V) produced high current/high power at breakdown voltage. Full OFF (V_G = -5.0 V) produced very small drain current (less than 5 microamps per micron) at breakdown drain voltage. Failure sites for all breakdown examples in this study were located in the channel region of the HEMT.

A. ON-state breakdown

Thermoreflectance imaging of pre-breakdown in the MOSHEMT in the full-ON state was studied for seven devices. Two distinct spatial thermal mechanisms showed correlation with the fail site during full ON operation. The first mechanism, which we will call case 1, manifests at high bias as a decrease in temperature in a region of the gate metal immediately followed by failure at the same location. This pre-breakdown thermal feature was observed in two of the seven MOSHEMTs imaged in the full-ON state. The second mechanism, case 2, showed a correlation between the location of small "cold spots" visible on the gate metal at low bias and the subsequent gate metal fail site at high bias. Case 2 was observed in two of the seven MOSHEMTs studied in the full-ON state. The remaining three MOSHEMTs in full-ON operation failed spontaneously at high bias and exhibited no correlation between local thermal features pre-breakdown and the eventual site of breakdown.

1) Temperature decrease at high bias: Fig. 2 shows one of the GaN MOSHEMTs which exhibited a localized decrease temperature on the gate metal at high bias with subsequent failure at the same location. Gate length is 2 microns. Fig. 2 (a) shows optical and thermal images of the gold gate metal for

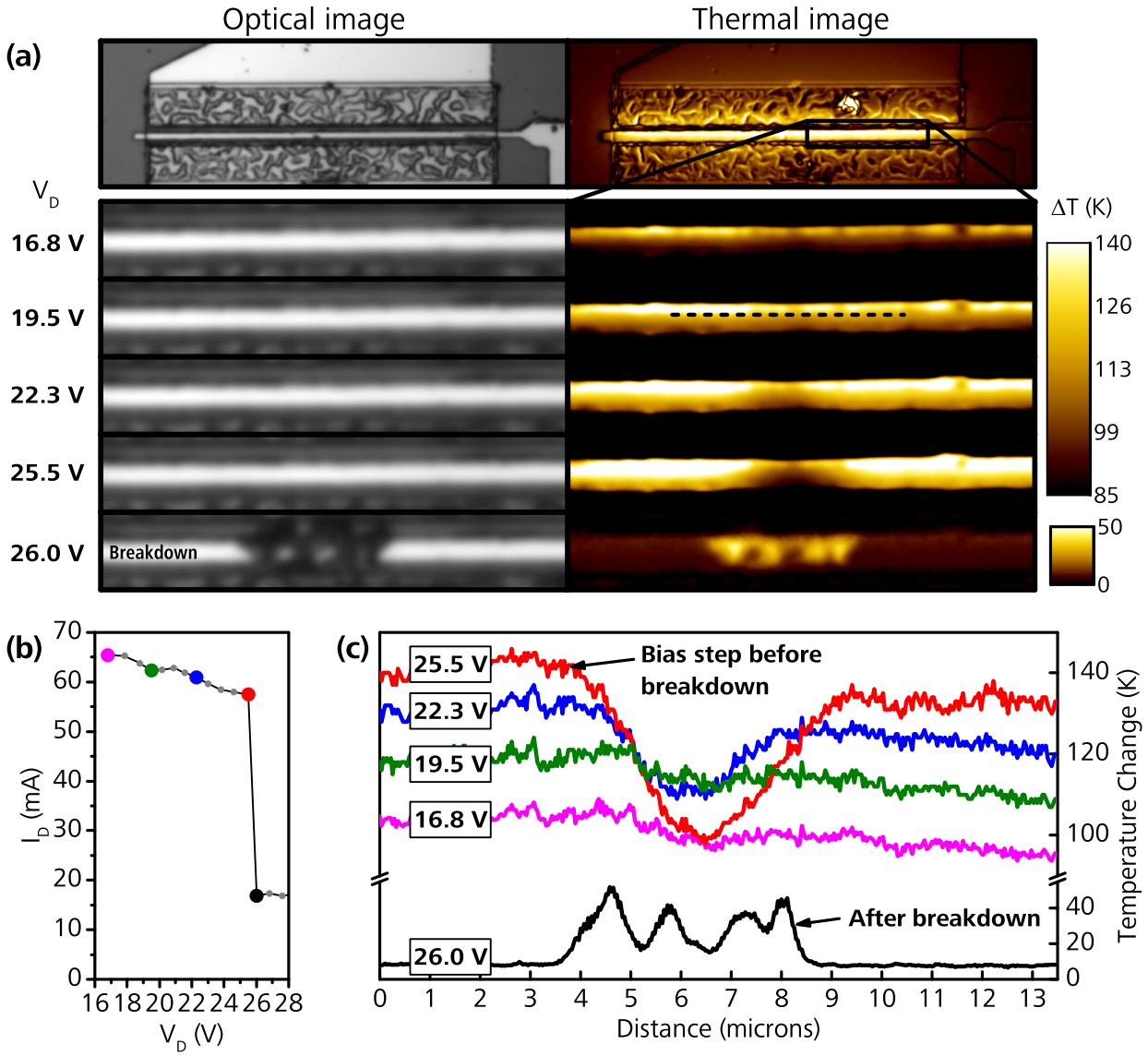

Fig. 2. (a) Optical and thermoreflectance images of MOSHEMT gate metal showing temperature drop in region of gate fail site for several drain voltage steps preceding device breakdown. Full ON operation (V_G = +2.0 V). Gate length is two microns. (b) I_D-V_D for each image. (c) Temperature change profiles on the gate metal fail site, sampled along the dashed horizontal line shown in the thermal image).

several voltage steps preceding breakdown. Magnified images highlight the region of the gate metal at which failure occurs. A local temperature anomaly first becomes visible at V_D = 22.3 V (I_D = 60 mA) as a local crescent shaped decrease in temperature near the source side of the gate metal. Evolution of the temperature profile along the gate metal (sampled along the indicated horizontal dashed line) plotted in Fig. 2 (c) Temperature decrease near the fail site becomes more severe with increasing bias, dropping by a maximum of 40% in the bias step immediately preceding breakdown at V_D = 25.5 V. Average gate temperature is 400 K. Catastrophic electrical breakdown occurs at the next bias step, V_D = V_{BR} = 26.0 V, represented by a 75% drop in drain current Fig. 2 (b). The location of the thermal anomaly coincides precisely with the fail site, visible as displaced gate metal (Au) in the optical image after breakdown. This result is surprising as failure in power devices at high bias is typically preceded by local increase in temperature (hotspots) rather than decrease. The localized temperature drop may indicate a depletion region in the channel where conductivity degrades with increasing power just prior to local failure. [5] It is worth noting from the thermal images at high bias there is a temperature gradient along the length of the gate, with the drain side hotter than the source side. This is consistent with electrical models that show HEMT potential is nonuniform along the length of the channel, with increased power dissipated on the drain side. The optical images show no change in the gate metal prior to breakdown, which confirms the measured thermoreflectance change is not skewed by changes in gate metal absolute reflectance.

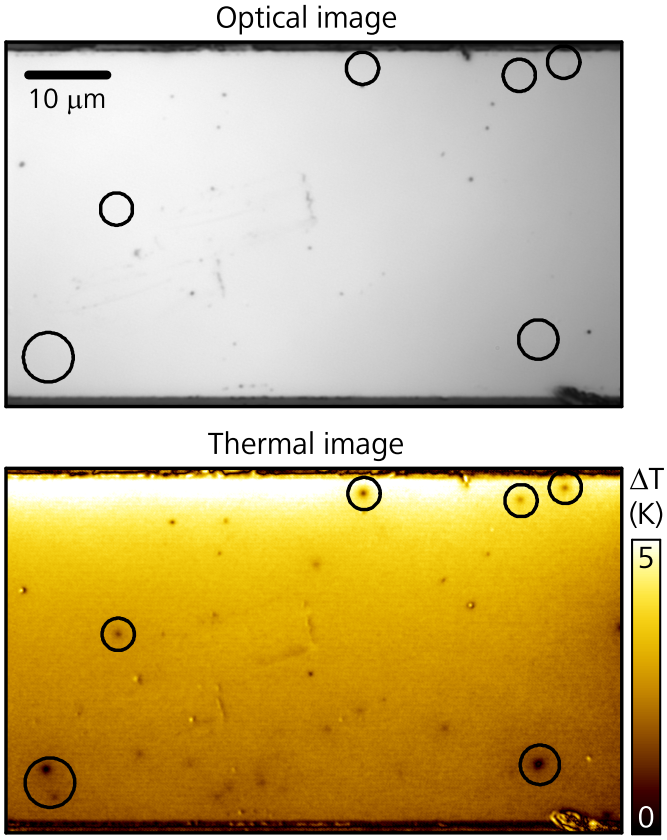

Fig. 3. Low bias cold spots in MOSHEMT gate metal under full-ON operation. V_G = +2.0 V, V_D = 4.2 V, I_D = 13 mA. Gate length is 40 microns.

2) Cold spots at low bias: The second distinct thermal mechanism observed in MOSHEMT pre-breakdown under full-ON operation manifested as highly localized cold spots visible on the gate metal at low bias. A correlation was observed between the location of these anomalous cold spots at low bias and the subsequent fail site at high bias. Fig. 3 shows optical and thermal images of a MOSHEMT with multiple cold spots distributed throughout the gate area. The device is in full-ON operation (V_G = +2.0 V) at low bias, V_D = 4.2 V, with I_D = 13 mA. Several conspicuous cold spots on the gate metal are indicated with circles in the thermal image, with corresponding locations in the optical image indicated. A MOSHEMT with large gate area (gate length = 40 microns) was selected to provide an overview of the distribution of cold spots across the gate surface. The size and spatial profile of a cold spot can be seen in Fig. 4 which plots the temperature change across two typical cold spots on the gate metal of one of the MOSHEMTS, this time for a shorter channel device with gate length = 4 microns, V_D = 1.2 V, and I_D = 9 mA. Cold spots were typically about one micron in diameter, though larger spots were observed. The cold spots have a nearly uniform radial shape. This is atypical in integrated electronics where self-heating features usually have an irregular shape. The consistent small size and spatial symmetry of individual

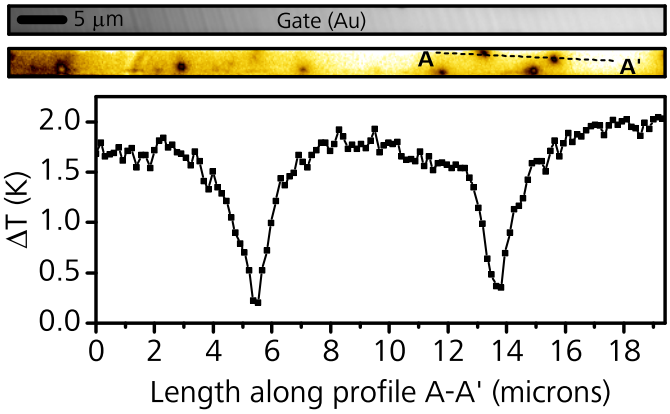

Fig. 4. Optical (top) and thermal (bottom) images of MOSHEMT cold spots on gate metal at low bias with temperature change across two spots plotted for indicated profile. Full-ON, V_G = +2.0V, V_D = 1.2 V, and I_D = 9 mA. Gate length = 4 microns.

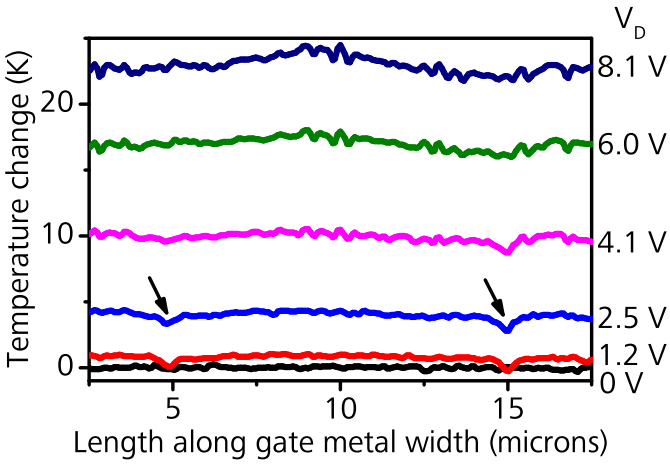

Fig. 5. Cold spot visibility for increasing bias. Temperature change profiles along MOSHEMT gate metal (thermal image in Fig. 4) for increasing drain voltage. Cold spots visible at low bias (arrows) become masked by overall gate heating at higher bias and power. Full ON, V_G = +2.0 V.

cold spots suggest their signal may originate from a effective point source that is smaller than the spot visible in thermal images. Fig. 5 plots evolution of cold spots and surrounding gate metal for increasing drain voltage sampled along the gate metal width of the MOSHEMT thermal image shown in 4 (using a profile different from the one plotted in that figure.) We observe the indicated cold spots at low bias (less than V_D = 2.5 V) are initially superimposed with the temperature profile of the adjoining gate metal. However with increasing bias and temperature the cold spots gradually become submerged in the wider self-heating distribution along the gate.

The cold spots exhibited several common characteristics. The cold spots are repeatable. The location, shape, and magnitude of the spots remained constant over successive thermoreflectance image measurements as long as the device was not stressed to breakdown. Applying high bias (V_D greater than 20 V) had no effect on subsequent images of the cold spots at low bias. Cold spots are present at low bias and

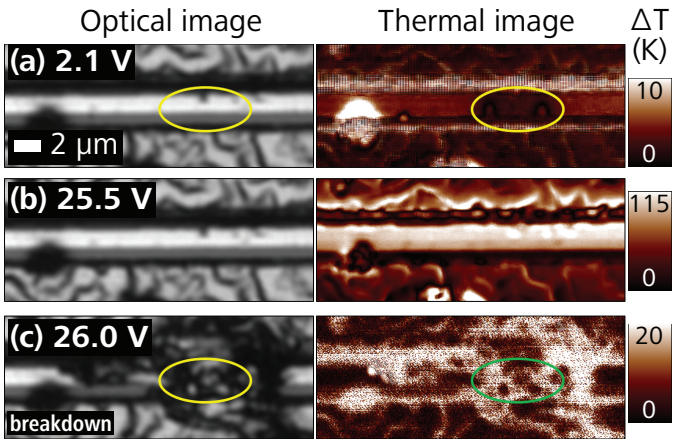

Fig. 6. Optical and thermoreflectance images of MOSHEMT gate metal showing colocated cold spots at low bias (a) and metal failure site following high bias breakdown (c). Cold spots are not visible at same location just before high bias breakdown (b). Full ON, V_G = +2.0 V.

power density (1 W/mm) and low average gate temperature (maximum temperature rise is less than 5 K) . This suggests the cold spots are present under nominal steady state operation and not the result of runaway electrical or thermal processes. Self-heating appears normal on the gate away from the cold spots. For example the temperature gradient along the gate length visible in the thermal image of Fig. 3 exhibits the expected increased self-heating on the drain (top) side of the gate. Electrical performance (I_D) did not show significant dependence on the presence or quantity of cold spots, but quantitative dependence will require testing a large number of MOSHEMTS. The cold spots are not measurement artifacts, as the optical image of the gate metal shows no surface defects or features at locations corresponding to cold spots in the thermal image.

Uniform local cold spots were present in five of the seven MOSHEMTs imaged during full-ON operation. When stressed to breakdown, two of these five displayed a correlation between the location of low bias cold spots and fail sites at high bias. An example of this breakdown correlation is shown in Fig. 6 for a MOSHEMT with gate length = 4 microns.) Fig. 6 (a) shows the optical and thermal images of the gate metal at low bias, V_D = 2.1 V, I_D = 9.5 mA, for V_G = +2.0 V. Temperature rise above ambient at this low power density is less than five degrees anywhere on the gate. (The bright spot on the gate in the thermal image is a measurement artifact caused by a region of discolored gate metal visible in the optical image.) Two uniform radial cold spots can be seen on the gate in the thermal image at low bias. The location of the cold spots in the thermal image and their corresponding location in the optical image are highlighted by circles. The optical image shows no defect in the gate metal top surface corresponding to the location of the cold spots, which suggests the cold spots are caused by a mechanism beneath the gate surface. Fig. 6 (b) shows the MOSHEMT at high bias, V_D = 25.5 V, I_D = 36 mA (9.2 W/mm). The cold spots present

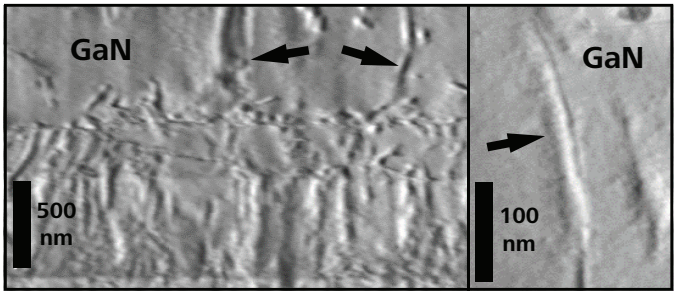

Fig. 7. TEM cross section images of MOSHEMT epitaxy showing possible vertical dislocations in the GaN layer.

in the thermal image at low bias are no longer visible in the thermal image at high bias. The MOSHEMT fails at the next 0.5 V step, shown in Fig. 6 (c). The optical image of the gate following breakdown shows metal deformation in the same location as the cold spots observed at low bias. Material deformation was not observed anywhere else along the gate. Although the number of MOSHEMTS stressed to breakdown in this study is not sufficient to conclude that the cold spots are linked to device failure, results motivate further study to explore a possible mechanistic relationship.

The origin of the cold spots is under investigation. One possible cause is the presence of static or transient defects that create local depletion regions in the conducting channel. Such a defect would manifest as an island of reduced power dissipation or a local cold spot. Cold spots that do not change over time or after multiple stresses could represent static defects in the bulk, thin film, or interface that arose during material growth or device lithography. [6] Fig. 7 shows transmission electron microscopy images of the MOSHEMT epitaxial GaN and buffer layers. The vertical threads indicate possible fixed microscopic dislocations in the GaN layer. When the MOSHEMT is electrically biased, these dislocations could give rise to local electric potential variations and local depletion regions. The very thin conducting layer in 2DEG structures may be especially sensitive to such defects. Dislocations due to lattice mismatch in GaN grown on silicon substrate and the role of these dislocations in vertical breakdown was studied by Knetzger etal. in 2016. [5] Cathodoluminescence imaging of GaN on silicon substrate revealed localized defects with similar size and distribution as the thermoreflectance cold spots. Another possible cause of the cold spots could be local defects occurring under bias due to hot electron trapping near active regions such as the GaN, buffer, or MgCaO gate dielectric layers. [7]–[9] Unlike material defects, hot electrons could manifest as transient defects that change magnitude or location over time. Traps in GaN based HEMTs have shown strong dependence on electrical pulse parameters and in some cases trap states can be reversed. [10] While none of the observed cold spots moved location, a subset did show small variations in the magnitude of measured thermoreflectance temperature change over time. Thermoreflectance identification of localized cold spots could

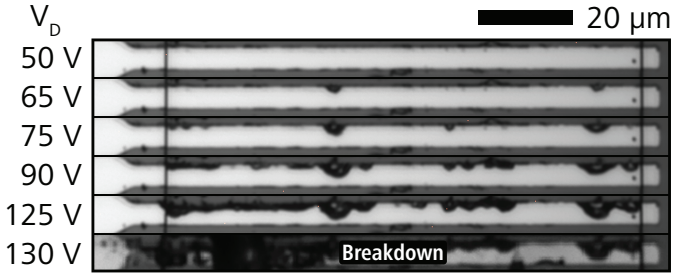

Fig. 8. Pre-breakdown under full-OFF operation (V_G = -5.0 V) for MOSHEMT with gate length of 6 microns. Optical images of gate metal for increasing drain voltage up to device breakdown at V_D = 130 V. Drain current is less than 0.1 mA for all images. Thermal images showed no temperature change.

provide new applications in reliability and integrated device material research. For example, the method could enable rapid, non-destructive, spatial characterization of electrically sensitive microscopic defects in HEMT structures. If cold spots are determined to indicate location and density of underlying bulk or thin film defects, the method can be generalized for rapid characterization of semiconductor materials. Future studies will investigate the relationship between the cold spots and MOSHEMT device performance across a large sample set. Measurement will compare areal fraction of cold spots visible on the gate to channel electrical resistance and breakdown voltage. TEM and SEM characterization of the device cold spot location may reveal possible bulk material causes. Transient electrical pulsing could probe the relationship between cold spot formation and hot electron trapping.

B. OFF-state breakdown

MOSHEMTs were also stressed to breakdown in the full-OFF state with V_G = -5.0 V. MOSHEMT performance and breakdown threshold while in the full-OFF state can be considered a measure of device voltage blocking capability. Typical full-OFF breakdown required V_D in excess of 130 V. Drain current was negligible, less than 100 microamps for all drain voltage levels. Images of MOSHEMT pre-breakdown in the full-OFF state suggested a fundamentally different mechanical process contributed to device failure compared to the full-ON case. Full-OFF pre-breakdown manifested as progressive deformation of the gate metal, principally on the high electric field drain side of the gate. Little or no self-heating was observed in the full-OFF state. Gate metal deformation is first observed as small blisters at the drain edge of the gate, typically beginning in the range of V_D = 50 to V_D = 90 V. As drain voltage increases, gate metal blistering gradually extends over more of the gate metal surface until catastrophic failure indicated by infinite channel resistance or no transistor switching capability. All six MOSHEMTs stressed to breakdown in the full$_{OFF}$ state displayed the same gate metal deformation characteristic. Fig. 8 shows optical images of pre-breakdown on the gate metal of a MOSHEMT stressed to breakdown under full-OFF operation. Gate length is 6 microns. Gate metal deformation first becomes visible at

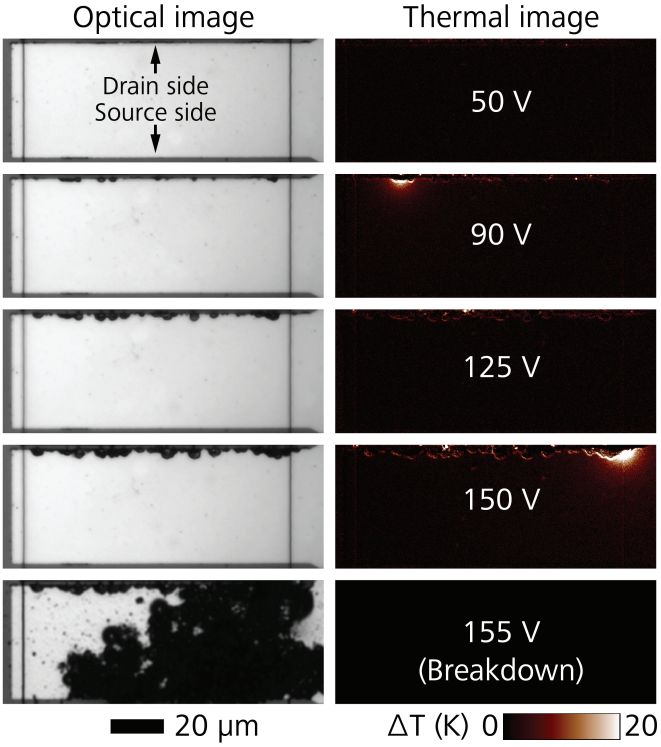

Fig. 9. Pre-breakdown under full-OFF operation for long channel MOSHEMT. Gate length = 44 microns.

V_D = 65 V and increases with drain voltage until catastrophic breakdown at V_D = 130 V. Thermal images are not shown because thermoreflectance images measured no temperature change on the gate over the full voltage sweep to breakdown. The same pre-breakdown characteristic under full-OFF was observed in a MOSHEMT with longer gate length (L_G = 44 microns) shown in Fig. 9. Again gate metal deformation begins on the drain edge of the gate and no deformation is observed on the source side. Sporadic, irregular heating was observed near the deformed gate metal for some of the voltage steps (V_D = 90 V, 150 V). However, the magnitude of heating (less than 20 K above room temperature) is nearly 100 K lower than temperatures at which the MOSHEMTs has demonstrated safe operation in the ON state.

CONCLUSION

High resolution spatial characterization of thermal, electrical, and mechanical effects in the pre-breakdown stages of GaN HEMT structures lends insight to the complex and often unintuitive underlying breakdown processes in power devices at high bias. The examples of GaN HEMT pre-breakdown under full-ON and full-OFF conditions demonstrate how thermoreflectance imaging microscopy can be used to study and improve HEMT reliability.

ACKNOWLEDGMENT

The authors would like to thank X.B. Lou and R.G. Gordon from Harvard University for their technical support on atomic layer deposition.

References

[1] S. Grauby, B. C. Forget, S. Hole, and D. Fournier, "High resolution photothermal imaging of high frequency phenomena using a visible charge coupled device camera associated with a multichannel lock-in scheme," *Review of Scientific Instruments*, vol. 70, no. 9, pp. 3603–3608, Sep. 1999.

[2] M. Farzaneh, K. Maize, D. Luersen, J. Summers, P. Mayer, P. Raad, K. Pipe, A. Shakouri, R. Ram, and J. A. Hudgings, "CCD-based thermoreflectance microscopy: Principles and applications," *Journal of Physics D: Applied Physics*, vol. 42, no. 14, p. 143 001, 2009.

[3] H. Zhou, X. Lou, N. J. Conrad, M. Si, H. Wu, S. Alghamdi, S. Guo, R. G. Gordon, and D. Y. Peide, "High-performance InAlN/GaN MOSHEMTs enabled by atomic layer epitaxy MgCaO as gate dielectric," *IEEE Electron Device Letters*, vol. 37, no. 5, pp. 556–559, 2016.

[4] X. Lou, H. Zhou, S. B. Kim, S. Alghamdi, X. Gong, J. Feng, X. Wang, P. D. Ye, and R. G. Gordon, "Epitaxial growth of $Mg_xCa_{1-x}O$ on GaN by atomic layer deposition," *Nano Letters*, vol. 16, no. 12, pp. 7650–7654, 2016.

[5] M. Knetzger, E. Meissner, J. Derluyn, M. Germain, and J. Friedrich, "Correlation of carbon doping variations with the vertical breakdown of GaN-on-Si for power electronics," *Microelectronics Reliability*, Sep. 2016.

[6] J. Brews, "Surface potential fluctuations generated by interface charge inhomogeneities in MOS devices," *Journal of Applied Physics*, vol. 43, no. 5, pp. 2306–2313, 1972.

[7] S. C. Binari, P. Klein, and T. E. Kazior, "Trapping effects in GaN and SiC microwave FETs," *Proceedings of the IEEE*, vol. 90, no. 6, pp. 1048–1058, 2002.

[8] G. Meneghesso, M. Meneghini, A. Tazzoli, A. Stocco, A. Chini, E. Zanoni, *et al.*, "Reliability issues of gallium nitride high electron mobility transistors," *International Journal of Microwave and Wireless Technologies*, vol. 2, no. 01, pp. 39–50, 2010.

[9] A. Asenov, R. Balasubramaniam, A. R. Brown, and J. H. Davies, "RTS amplitudes in decananometer MOSFETs: 3-D simulation study," *IEEE Transactions on Electron Devices*, vol. 50, no. 3, pp. 839–845, 2003.

[10] J. Franco, B. Kaczer, N. Waldron, P. J. Roussel, A. Alian, M. A. Pourghaderi, Z. Ji, T. Grasser, T. Kauerauf, S. Sioncke, *et al.*, "RTN and PBTI-induced time-dependent variability of replacement metal-gate high-K InGaAs FinFETs," in *Electron Devices Meeting (IEDM), 2014 IEEE International*, IEEE, 2014, pp. 20–2.